Improving Catalytic Activity and Reuse for Palmitic Acid Aromatization in the Presence of Supercritical Water

Joseph Esposito, Jeffrey Page, Philip Smolitsky, Douglas Theberge

Chemical Engineering MQP 2019-2020

Advisor: Dr. Michael Timko

Abstract

ZSM-5 has been investigated for promoting conversion of palmitic acid to aromatics in the presence of a supercritical water phase at concentrations lower than previously studied. The rate of palmitic acid decomposition is roughly 50× greater than comparable previous reports. The catalyst was reused four times with modest activity loss after the first cycle and negligible loss for all subsequent cycles. Post-reaction characterization of ZSM-5 revealed less degradation than previously reported. Time studies and control experiments in the absence of catalyst were used to elucidate the thermal and catalytic contributions to the product distribution. The current study opens new avenues for catalytic upgrading of renewable oils in the presence of supercritical water.

Table of Contents

Introduction

Petroleum is the primary source of liquid transportation fuels and chemical feedstocks used to produce polymers, commodity and specialty chemicals, and pharmaceuticals. While much focus has been on replacement of petroleum for production of gasoline, diesel, and jet fuel [1], the transition to a sustainable bio-economy requires replacing petroleum with renewable sources [2, 3]. One of the most important industrial feedstocks are the "BTEX" compounds, benzene, toluene, ethylbenzene, and xylene. BTEX compounds are used for solvents, dyes, paints, and plastics applications, all of which are more valuable than use as a fuel. Accordingly, co-production of BTEX compounds from renewable sources has potential to improve the economics of biofuel production [4].

Catalytic cracking of oils derived from waste and renewable sources has recently attracted interest for production of chemicals, especially in the BTEX family [5-11]. Zeolites, specifically ZSM-5, have been proposed by several researchers for this purpose, owing to their selectivity toward single-ring aromatics [5-11]. Unfortunately, zeolites suffer from catalyst deactivation, largely attributed to coke formation, which hinders their long-term use in commercial applications [12-14]. Specific to fatty acid aromatization, Taufiqurrahmi et al.[15] reported that zeolite coking led to rapid catalyst deactivation for cracking of palm oil to aromatics. Accordingly, questions remain about ZSM-5 reusability and coking, despite repeated reports on its use [8, 16-22].

Recent work has shown the presence of water in a liquid or dense supercritical phase inhibits coke formation on ZSM-5. Zaker et al. [23] found that co-feeding dodecane and water in equal mass fractions (50 wt%) decreased coke formation by >10 times relative to that observed in the absence of water. Guerra et al. [24] reported that water inhibited conversion of single-ring aromatics to form multi-ring molecules associated with hard coke. The inhibition

effect of water was attributed partially to direct participation of water in the coke formation mechanism. Similarly, Zaker et al. [23] studied the water-dodecane reaction mechanism in the presence of ZSM-5, finding that the presence opened new pathways of low-temperature hydrocarbon reformation and coke gasification that prevented coke accumulation on the surface. These findings suggest that supercritical or dense liquid water phases can extend ZSM-5 lifetime when used for catalytic conversion of renewable oils to BTEX compounds. From a practical standpoint, water is a common contaminant that requires energy intensive processes to remove [25].

Unfortunately, water deactivates zeolites by mechanisms other than coke formation, leading to irreversible loss of activity [26-28]. Despite being known for its relative stability among zeolites [29], ZSM-5 decrystallizes and dealuminates in the presence of liquid and supercritical water [26-28] prompting questions about the practicality of the water-assisted approach to coke suppression. Previous reports on the reuse of zeolites in the presence of liquid water have yielded mixed results [27, 28, 30, 31].

Maag et al. [26] studied ZSM-5 decrystallization and dealumination in liquid water over a wide temperature range, providing suggestions to extend ZSM-5 stability. ZSM-5 decrystallization rate exhibits a local minimum at temperatures slightly greater than the critical point (374 °C). The observed minimum was attributed to the depletion of H_3O^+ and OH^- at supercritical conditions, a phenomenon associated with the well-studied temperature dependence of K_w and consistent with previous models of acid and base promoted zeolite degradation [26, 32-34]. Accordingly, operation at temperatures that minimize decrystallization was suggested as well as addition of a less aggressive co-solvent to dilute acids and bases to extend ZSM-5 stability in the presence of liquid water [26]. Since few co-solvents are expected to be stable in the presence of supercritical water and ZSM-5 [35], an

alternative to co-solvent addition is use of a reaction mixture consisting primarily of non-polar reactants and a minority water phase [26].

To date, the non-polar dilution strategy has not been studied explicitly, as the majority of zeolite-catalyzed aromatization studies in the presence of water have used reaction mixtures consisting of >50 wt% water [31, 36]. As a result, questions remain about the ability of minority water components to suppress coke and the ability of non-polar components of the reaction mixture to reduce zeolite degradation. Similarly, the relative importance of catalytic and thermal cracking and aromatization pathways is not clear [31]. Answering these questions will therefore be an important contribution to this field.

Here, we study ZSM-5 catalyzed palmitic acid cracking in the presence of a minority water component (15 wt%) under single fluid phase conditions at 400 °C and 22±2 MPa in a batch reactor. Palmitic acid was selected as a model reactant due to its abundance in used cooking oil and microalgae.[15, 22, 37] ZSM-5 was selected as a commercial zeolite with known BTEX formation activity and with greater stability in the presence of liquid water than other commercial zeolites [28]. Reaction conditions were selected to ensure that palmitic acid, water, and primary reaction products formed a thermodynamically stable single phase, thereby eliminating uncertainty stemming from fluid-fluid interfaces [38]. Catalyst activity, selectivity, and reuse were examined and compared with previous reports on palmitic acid cracking in the presence and absence of water in the reaction mixture. Catalyst reuse tests were performed (4 cycles) and used catalysts were characterized for signs of degradation. Lastly, time study data and comparison with product distributions obtained under thermal conditions were used to propose a possible thermo-catalytic mechanism. These results suggest water as a new strategy for managing catalyst deactivation while converting renewable and waste oil feeds into valuable chemicals.

Materials and Methods

Materials

Palmitic acid with a purity of 98% was acquired from Acros Organics (p/n AC129700010). Nano-HZSM-5 was obtained from ACS Materials with a silica-to-alumina atomic ratio of 26. Fresh catalyst was dried in an oven at 100 °C for 3 h before being calcined (550 °C for 15 h) to remove template material. Water was de-ionized to a minimum resistivity of 17.9 MΩ·cm immediately prior to use. ACS reagent grade dichloromethane (CH_2Cl_2, DCM) was obtained from Pharmco-AAPER at 99.8% purity. ACS reagent grade acetone (C_3H_6O) was obtained from Fisher chemical at 99.5% purity. n-heptane (C_7H_{16}) was obtained from Acros Organics at 99+% purity. HPLC grade methanol was obtained from Sigma-Aldrich at 99.9% purity. D-chloroform was purchased from Cambridge Isotope Labs (p/n DLM-7TB-100S) with a purity of 99.8% and a TMS of 0.05%. Compressed nitrogen, helium, hydrogen and air (99.999% purity) were obtained from Airgas.

Reaction Experiments

Reactions were conducted in a 100 cm^3 stainless steel Parr batch reactor (p/n 4590 micro) equipped with gas inlet and release valves, a 0–35 MPa pressure gauge (p/n 593HCP50AD) and a rupture disk (p/n 526HCP50CTYZ50) for safety. A Parr magnetic drive (p/n A1120HC6) and stainless-steel stirring rod were used to control mixing within the reactor. An electric heating jacket (Parr Instrument, p/n A3240HC6EB) was used to heat the reactor to a desired temperature based on readings from a thermocouple (p/n A472E2) within the reactor. Temperature and stirring rate were set using a reactor controller (Parr Instrument, p/n 4848). A reaction and analysis schematic can be found in Figure S1 in the appendix.

For all reactions, 8.00 grams of palmitic acid (PA), 0.40 grams of ZSM-5 (5 wt% relative to the initial PA loading), and 1.41 grams of DI water (15 wt% relative to the initial PA loading) were placed within the reactor. After loading reactants, nitrogen gas was fed to the reactor (~3.4 MPa) and vented at least five times to purge it of air prior to reaction. Finally, the reactor was pressurized to 9 MPa with nitrogen gas to ensure the reaction reached supercritical pressure (23 ± 1 MPa) and heated to the desired temperature (for most reactions 400 °C). The reaction temperature was held for a specified duration ranging from 0 to 90 minutes, after which the reactor was removed from the heater and quenched in a water bath. All experiments were carried out at least twice to evaluate reproducibility and most tests were repeated between 3 and 6 times.

Catalyst re-use experiments were conducted for the 30-minute reaction, chosen as it was the shortest reaction to reach ~100% conversion. Catalyst was collected from several 30-minute reactions and de-coked in air for 15 hours at 550 °C. This “replenished” catalyst was analyzed according to methods found in the appendix. Remaining catalyst was used to conduct a subsequent cracking reaction with the same conditions (30 minutes, 400°C, 23 ± 1 MPa, 15 wt% water, 5 wt% ZSM-5). This process was carried out until the catalyst had depleted from usage, and four re-use reactions were conducted. These re-use runs were labelled ‘Fresh’ for reactions with catalyst which had not been previously used and ‘Cycle X’ for reactions with catalyst de-coked after X reactions. Each re-use cycle was conducted at least twice except for the final re-use (due to depletion of catalyst) to ensure reproducibility of data.

Product Analysis

After reaction, the gas collected in the reactor was vented through a gas chromatograph (GC) sample loop for quantification. The reactor was opened, and the oil product recovered and analyzed by a separate GC and (for representative samples) proton nuclear magnetic resonance

(NMR). Solids were removed by filtration and stored for further analysis. Detailed analysis procedures of the various phases are described in the following sections.

During reactions, reactor temperature and pressure as well as reaction time were recorded. Experiments with procedural outliers (obvious gas leaks, slow temperature ramp, et cetera) were immediately disqualified for analysis. Reactor leaks were tested for before reactions by holding initial pressure of 9 MPa for 1-2 minutes, and after infrequently by weighing the gas-phase product.

Gas-phase products were analyzed with a GC (GC-2014 Shimadzu system) equipped with a thermal conductivity detector (TCD) an 80/100 Hayesep Q packed column (3 m × 0.125 in × 2.1 mm SS). The carrier gas was helium with a flow rate of 10 sccm. The initial temperature was 30 °C, and which was increased at rate of 5 °C min^{-1} until reaching 90 °C, after which the temperature was held for 20 minutes. The TCD temperature was set to 150 °C and the current was set to 120 mA. Gases were identified by retention time matching with known standards and TCD response areas were converted into concentrations using calibrated response factors. Residence times and response factors were determined for the following compounds: CO_2, CH_4, C_2H_4, C_2H_6, C_3H_8, C_4H_{10}, C_5H_{12}, and C_6H_{14} using calibration standards. Different isomers of C4 through C6 compounds were unable to be distinguished, and for this reason the relative ratios of the isomers were assumed to be the same as the oil phase for analysis.

Hydrogen and CO could not be directly quantified using this method, as these gases co-eluted with the nitrogen that was used to pressurize the reactor before each run. For several representative runs, the reactor was pressurized with helium for qualitative identification of hydrogen in the product gases.

For analysis, the oil and water phases separated under gravity and the supernatant oil phase was filtered and diluted with DCM in a recorded ratio (typically 1/100). This solution was analyzed using a GC equipped with a quadrupole mass spectrometer detector (MS, QP

2010 SE system, Shimadzu) for product identification and a flame ionization detection (FID, Shimadzu) for quantification.

For GC-MS, the column was SHRXI-5MS (30 m×0.25 mm ID×0.5 μm film thickness), and for FID the column was Rt-Q-BOND (30 m×0.25 mm ID×8 μm film thickness). The same temperature program was used for both FID and GC-MS: the initial column temperature was 35 °C and the column temperature increased at 3°C min^{-1} until reaching 290 °C, at which point the temperature was held constant for 5 minutes before completion. The injector temperature was 300 °C and the injected sample volume was 3 μl. FID response factors were determined using hexane, heptane, octane, decane, dodecane, hexadecane, toluene, o-xylene, ethylbenzene, 1,2,4-trimethylbenzene, 1-methylnaphthalene and palmitic acid and generalized using the method described by Perkins et al. [39]. Yields were calculated on a mole and mass basis using FID areas, response factors, and initial PA loading.

The aqueous phase was separated, weighed, and not analyzed further. Analysis was not conducted for a variety of reasons. Mass and carbon balance closure throughout reactions was nearly complete, indicating negligible loss of carbon to the aqueous phase and consistent with the expected partitioning behavior of the hydrocarbons that constituted the majority of the products. Similarly, previous work by Zaker et al. [23] reported <1 ppm carbon content in the aqueous phase after reaction.

GC analysis was able to quantify approximately 80-100% of the individual oil products formed after PA reaction. The remainder of the product mixture was not sufficiently volatile for GC elution. To characterize these products, oil products from a range of reactions were placed in vials with the lids removed at room temperature to evaporate to dryness over a three-week period. The resulting oil, comprised of relatively non-volatile “heavy” compounds, was dissolved in d-chloroform, and H NMR spectra were acquired using a Bruker BioSpin 500MHz Avance AV-III Digital NMR spectrometer.

Solids were separated from the oil by vacuum filtration followed by washing the solids with water and DCM until the solvent passing through the filter was clear. Coke was then placed in a 60 °C oven overnight to remove excess DCM. Temperature programmed oxidation (TPO) of the washed and dried solids was performed using a Netzsch model 209 F1 Libra TPO instrument to remove and/or quantify coke. For each experiment, a 60-70 mg portion of the sample was placed in an alumina crucible that was then loaded into the TPO instrument. The temperature was then increased from ambient to 800 °C at a ramp rate of 10 °C min^{-1}. Oxygen and nitrogen flow rates were set to 4 and 8 mL min^{-1}, respectively. TPO tests were performed in duplicate for representative samples and all features were found to be reproducible within 11%.

Product yields were determined on a compound-by-compound basis. Yields estimated for individual compounds were then used to check the carbon, hydrogen, and oxygen balances. For the various reaction durations, carbon closure averaged 91% ± 4% for 0-15 min and 96% ± 2% for 30-90 min. Carbon balance improved as conversion reached 100% since the major contribution to carbon loss was as palmitic acid that could not be recovered quantitatively from the reactor. Overall mass balance closure averaged 84% ± 3% for all reactions conducted. For the 30-minute catalyst cracking products, ~0.15 mol O/mol O fed was contained within observed products (mostly CO_2). Previous work by Class et al. [40] suggests that the majority of CO_X products formed within our reaction conditions should be present as CO_2 due to the water-gas-shift reaction. Further, oxygenation would not be expected in coke formation or within "heavy products"—those unable to be vaporized within our gas chromatograph. Therefore, assuming leftover oxygen to close the balance forms only water, our experiment forms at most 58.3 mmol of water. In the 30-minute reaction, the 0.16 mol of leftover hydrogen, reduced to 47 mmol H accounting for water formation, may form heavy compounds and/or hydrogen gas. Assuming heavy products have a carbon to hydrogen ratio of 1:1, only 14.7

mmol H may be contributed to heavy compounds before closing the carbon balance. Therefore, we may roughly estimate that, according to our assumptions, 16 mmol of hydrogen gas forms. While assumptions on CO yield may deviate from reality, this analysis shows that leftover yields for oxygen, carbon, and hydrogen can be reasonably explained with products which were unable to be detected and quantified within our experimental set-up.

Catalyst Characterization

Catalyst characterization was performed using X-ray powder diffraction (XRD), Fourier Transform Infrared Spectrograph (FT-IR), N_2 adsorption isotherm analysis, and Scanning Electron Microscopy (SEM). Detailed descriptions of the characterization methods are included in the appendix. The same catalyst used in the reuse experiments was used for catalyst characterization. The catalyst was de-coked before characterization following the same de-coking procedure outlined in the catalyst re-use experiments section above.

Results and Discussion

The objective of this work was to examine the promotional effect of dense liquid or supercritical water on palmitic acid cracking catalyzed by ZSM-5. The results are presented in three sections: 1) activity and product analysis tests, 2) catalyst stability and reuse testing, and 3) reaction pathway analysis.

Activity and Product Analysis

The first set of experiments consisted of evaluation of palmitic acid cracking catalyzed by ZSM-5 in the presence of dense, liquid-like or supercritical water. Reaction conditions were selected (400 °C and 23 ± 1 MPa) to ensure presence of a thermodynamically stable single fluid phase at all conversions from 0 to 100%, following the thermodynamic modeling of hydrocarbon-water mixtures at similar conditions presented previously by He et al. [38]. Operation under single fluid-phase conditions eliminates uncertainty associated with fluid-fluid mass transport limitations. While water as a pure substance would be in its supercritical state at the selected reaction conditions, as a mixture the supercritical state is no longer clearly defined thermodynamically [41]. At 400 °C and 23 ± 1 MPa, water is present in a dense, liquid-like form that approximates its supercritical state [42]. Accordingly, water is described in this work as being in its supercritical state, following standard convention [41].

For each experiment, reactant and reaction products were recovered and quantified. **Table 1** summarizes yields of all major products (i.e., any product with a molar yield greater than 0.05 relative to the initial moles of palmitic acid charged to the reactor), categorized as palmitic acid (PA), CO_2, C_1-C_3 gases, aliphatics, and aromatics.

Table 1. *Molar yield of products (mol of product per mol of palmitic acid) over a range of reaction durations and at several temperatures.*

Products (mol/mol PA)	0 min, 350ºC	0 min, 400ºC	15 min, 400ºC	30 min, 400ºC	45 min, 400ºC	90 min, 400ºC
CO_2	0.07 ± 0.03	0.03 ± 0.03	0.11 ± 0.04	0.12 ± 0.03	0.11 ± 0.04	0.08 ± 0.02
Total C_1-C_3	0.09 ± 0.04	0.06 ± 0.03	0.21 ± 0.07	0.24 ± 0.06	0.21 ± 0.05	0.24 ± 0.02
C_4	0.23 ± 0.04	0.42 ± 0.10	0.56 ± 0.22	0.58 ± 0.06	0.52 ± 0.12	0.47 ± 0.02
C_5	0.26 ± 0.06	0.48 ± 0.07	0.52 ± 0.09	0.50 ± 0.04	0.50 ± 0.08	0.36 ± 0.02
C_6	0.21 ± 0.16	0.22 ± 0.04	0.24 ± 0.05	0.21 ± 0.04	0.20 ± 0.05	0.16 ± 0.02
C_7	0.06 ± 0.00	0.09 ± 0.01	0.08 ± 0.01	0.06 ± 0.01	0.07 ± 0.01	0.07 ± 0.01
C_8	0.06 ± 0.01	0.07 ± 0.01	0.07 ± 0.01	0.06 ± 0.00	0.07 ± 0.00	0.06 ± 0.02
Total Aliphatics	0.86 ± 0.12	1.35 ± 0.15	1.54 ± 0.23	1.46 ± 0.08	1.39 ± 0.14	1.17 ± 0.02
Olefin/Paraffin	1.32 ± 0.34	1.09 ± 0.12	1.03 ± 0.06	0.52 ± 0.10	0.65 ± 0.09	0.54 ± 0.17
Benzene	0.01 ± 0.00	0.02 ± 0.00	0.02 ± 0.00	0.03 ± 0.00	0.03 ± 0.00	0.04 ± 0.01
Toluene	0.06 ± 0.00	0.10 ± 0.01	0.11 ± 0.02	0.17 ± 0.01	0.14 ± 0.01	0.18 ± 0.03
Ethylbenzene	0.02 ± 0.00	0.04 ± 0.00	0.04 ± 0.01	0.06 ± 0.00	0.05 ± 0.00	0.06 ± 0.01
Xylene	0.10 ± 0.01	0.15 ± 0.01	0.17 ± 0.03	0.23 ± 0.01	0.21 ± 0.01	0.25 ± 0.03
Total Aromatics	0.39 ± 0.06	0.63 ± 0.05	0.69 ± 0.11	0.91 ± 0.04	0.86 ± 0.05	1.06 ± 0.06
PA Conversion	0.60 ± 0.01	0.92 ± 0.02	0.97 ± 0.02	> 0.998	> 0.998	> 0.998

Conditions: 5 wt% ZSM-5 (relative to palmitic acid), 15 wt% water, 23 ± 1 MPa, and reaction temperatures and times as indicated.

Palmitic acid conversion increased with increasing reaction time and reaction temperature, as expected. At 400 °C, PA was detected only when the reaction time was ≤15 min. For all other reaction times, PA concentrations in the product mixture were less than the detection limit and the corresponding conversion could only be estimated as >0.998.

CO_2 was a major product under most conditions and its yield generally increased with PA conversion. The major source of CO_2 is PA decarboxylation [31, 43] (Mo et al., Santos et al.)]. CO could not be quantified separately; however, previous work by Class et al. [40] suggests that the majority of CO_X products formed under the reaction conditions used here should be present due to the water-gas-shift reaction. Yields of C_1-C_3 gases were similar to those observed for CO_2.

Hydrocarbons were the primary reaction product at all times. Both paraffins and olefins were formed, and C_4 and C_5 compounds were the most abundant aliphatic products. This observation indicates rapid cracking of the C_{16} carbon chain of palmitic acid into smaller

fragments. The olefin-to-paraffin ratio generally decreased with increasing PA conversion, consistent with olefin formation as a primary product of decarboxylation and PA cracking reactions followed by subsequent saturation or cyclization.

Aromatic yields increased over time, starting at 0.63 ± 0.05 for the shortest reaction time and increasing to >1 mol mol^{-1} after 90 min. Interestingly, aromatic yields continued to increase after PA conversion had reached completion, indicating formation of aromatic products by secondary reactions involving paraffins and/or olefins. Independent of PA conversion, toluene and xylene were the most abundant one-ring aromatics. In general, yields of two-ring aromatics were an order of magnitude less than the one-ring aromatics, as desired from an economic perspective.

Aside from the compounds shown in Table 1, coke and heavy products were also formed. Coke was determined by the difference in mass observed after oxidation of recovered catalysts. TPO thermographs are provided in **Figure S6** in the Appendix. Heavy compounds were classified as those that could not be volatilized and detected in the oil-phase GC analysis (290 °C). Heavy products were analyzed using ^{1}H-NMR after first allowing the oil to vaporize at room temperature for several weeks from an open vial.

Coke yields were measured at 30 min of reaction time at 400 °C with 15 wt% SCW as 2.6 mg g^{-1} PA, showing a ~4x reduction from a 12.2 mg g^{-1} PA coke yield without SCW measured from two reactions conducted at identical conditions without added water. Accordingly, coke formation occurred rapidly, consistent with a previous report by Zaker et al. [23]. Visually, the appearance of the recovered catalyst progresses from brown to black with increasing reaction time, consistent with its conversion from aliphatic soft coke to aromatic hard coke, as previously observed by Guerra et al. [24].

The heavy products were analyzed using ^{1}H-NMR as a volatility-independent method to evaluate composition. **Figure S3** in the Appendix provides the raw ^{1}H-NMR spectra. In

summary, ^{1}H-NMR indicates that the heavy products are composed of polycyclic aromatic hydrocarbons and/or aromatics bearing aliphatic side chains. The formation mechanism is therefore cyclization followed by sequential dehydrogenation to form the aromatic cores, followed by alkylation to from the aliphatic side chains.

A major objective of this study was to determine the effect of a minority water component on ZSM-5 catalyzed fatty acid cracking under supercritical conditions. To evaluate this effect, the current data were compared with several data sets reported in similar literature studies [5, 6, 8, 10, 31]. **Table 2** summarizes the comparison. The most direct comparison is with Mo et al. [31], with the main difference being the initial water loadings used in the two studies (66 wt% compared with 15 wt% in the current study). In both cases, aromatic selectivity was comparable (35 vs. 39 mol%). Interestingly, however, after accounting for differences in PA conversion and catalyst loading, the estimated reaction rate observed in the current study is 65-times greater than that reported by Mo et al. [31]. Accordingly, reducing initial water loading increases PA cracking rates without sacrificing aromatic selectivity. Although Mo et al. [31] did not report coke yields, the coke yields observed here (<1 wt%) are much less than have been reported previously for catalytic pyrolysis in the absence of liquid water.

Table 2. *Comparison to values from other fatty acid cracking studies with ZSM-5 [5, 6, 8, 10, 31]. A '-' is used to indicate that the data was not reported in the study*.

Reference	Feed	Reaction Conditions (Temp / Pres / Time)	Cat. Loading (g/g PA)	Water Loading (wt%)	Conversion (%)	Coke Yield (wt%)	Aromatic Selectivity
This Work	**PA**	**400°C / >22.1 MPa / 30 min**	**0.05**	**15**	**~100**	**0.26**	**48 wt% (35 mol%)**
Mo et al.	PA	400 °C/ >24 MPa / 25 min	1.00	66	43	-	39 mol%
Emori et al.	Soybean Oil	450°C / 0.1 MPa / 45 min	0.33	0	~100	-	22-40 wt%
Katikaneni et al.	Canola Oil	400°C / 0.1 MPa / 30 min	1.11	25	93	2.0	41 wt%
		400°C / 0.1 MPa / 30 min	0.56	25	92	3.0	42 wt%
Botas et al.	Rapeseed Oil	550°C / 0.1 MPa / 60 min	0.13	0	~100	-	34 wt%

Twaiq et al.	Palm Oil	400°C / 0.1 MPa / n/a	0.40	0	97	1.7	38 wt%

In addition to the comparison with the study reported by Mo et al. [31], **Table 2** provides several other useful comparisons with fatty acid cracking catalyzed by ZSM-5 at atmospheric pressure. While studies at atmospheric pressure evaluated more complex feeds than PA which prevents direct comparison with the results obtained here, Table 2 shows that fatty acid cracking in the presence of supercritical water results in similar aromatic selectivity compared with previous reports, with similar conversion at similar reaction times while using less catalyst and while co-producing less coke (when quantified).

All of these considerations indicate that fatty acid cracking in the presence of a minority water component confers the coke reduction benefits of supercritical water, while increasing cracking rates and without sacrificing aromatic yields. Previous work on the use of catalysts in the presence of supercritical water has reported mixed results on catalyst lifetime, regenerability, and regenerability [31]. Accordingly, the next step of this study was testing catalyst reusability.

Catalyst Stability and Reusability

To test the reusability of the ZSM-5 catalyst, a sequence of reactions was performed at standard conditions (30 minutes at 400°C). Catalyst was recovered after each reaction, regenerated by removing coke, and reused. In total, catalyst activity was evaluated for 4 cycles. Of all of the products, aromatic yields are the best indicator of catalyst performance after regeneration. Accordingly, **Figure 1** provides aromatic yields and selectivity observed for each of the 4 cycles. All experiments were performed at least in duplicate, with error bars shown, except for cycle 3, which was performed only once. Based on the uncertainties of the rest of the data, the uncertainty in yields obtained after cycle 3 are <5%.

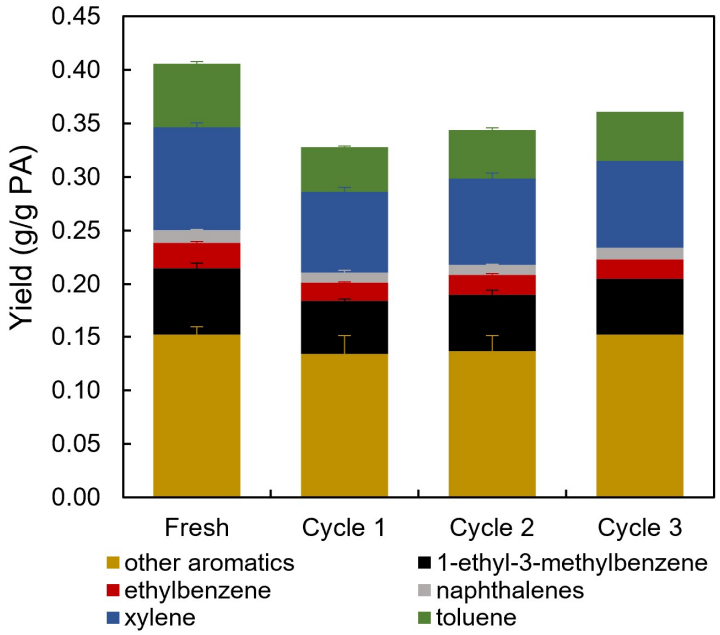

Figure 1. *Comparison of aromatic yield between cycles of catalyst use. Catalyst was de-coked after use for 15 hours in air. Reactions are labeled by the catalyst used for the reaction. Reaction conditions: 30-minutes, 400°C, and 23 ± 1 MPa.*

Figure 1 shows that aromatic yield decreases after first catalyst reuse by approximately 20%, with aromatic yield then gradually increases with each successive use. Cycle 3 retains 88% of the aromatic yield observed for the fresh catalyst. For comparison, previous studies with more abundant water components in the reaction mixture report that aromatic yield decreased by 40% after three use-reuse cycles [31].

Activity tests shown in **Figure 1** provide a strong indication of the reusability of ZSM-5 under the current reaction conditions. For commercial use, a typical figure of merit is that a catalyst must remain active for >1,000 h. Since performing activity tests for 1,000 h is not practical at lab scale, the used catalysts were recovered and evaluated for signs of degradation using x-ray diffraction (XRD) to monitor changes in crystallinity, N_2 sorption to study texture properties, and infrared (IR) spectroscopy to evaluate chemical changes.

Zeolite crystallinity retention is a common way to quantify degradation in hot liquid and supercritical water [44, 45]. In particular, Zaker et al. [23] showed that retention of crystallinity was required for retention of zeolite activity. Representative XRD patterns for each reuse cycle can be seen in **Figure 2**. The sharp diffraction peaks from 23-25 2θ degrees associated with the MFI framework of ZSM-5 are visible after every cycle, suggesting that crystalline structure is at least partially retained after four cycles of use. Moreover, no new peaks appear after use, indicating that no new crystalline phases form at reaction conditions.

To quantify the crystallinity change, ASTM Standard D5758 [46] was used to integrate the area under the XRD curve and compared with the value obtained for the fresh catalyst. This standard has been found to be reproducible within 3% and has a 95% confidence interval of ±5.04% [46]. Crystallinity values are provided directly in **Figure 2** for reference. In all cases, ZSM-5 retained ≥90% of its initial crystallinity, with most of the change occurring between the first and second use. After the initial decrease, crystallinity reaches a stable value of approximately 90%. This suggests that ZSM-5 may consist of some regions that are vulnerable to amorphization. Once these are removed, the remaining material is stable to further amorphization.

In comparison with the results obtained from using ZSM-5 in the presence of a minority water component (15 wt%), Zaker et al. [23] reported that the crystallinity of ZSM-5 used in a reaction mixture containing 50 wt% water decreased by >20% after a single use, establishing that the current conditions are much less aggressive.

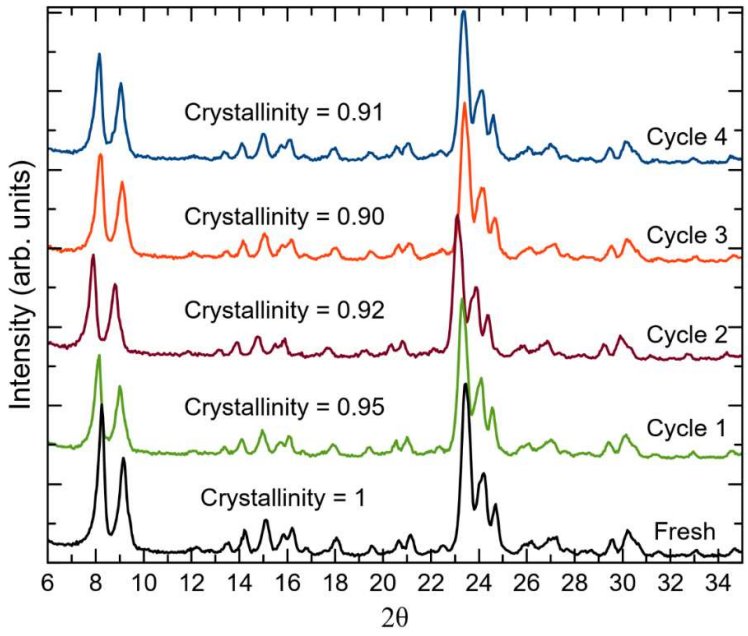

Figure 2. *XRD patterns of fresh and regenerated ZSM-5. The corresponding degree of crystallinity is calculated using the ASTM Standard D5758 [46].*

Used catalysts were tested using N_2 adsorption to evaluate effects on textural properties, Table 3 summarizes the results. After the first two uses, micropore area decreases by 21% and micropore volume by 13% relative to values measured for the native material. In subsequent cycles (three and four), these properties then remained constant. Micropore area decreases by 21% of the fresh catalyst over initial two uses before clearly stabilizing. Estimated external surface area followed a similar pattern, and the overall conclusion is that the catalyst shows no signs of irreversible deactivation after 4 use-regeneration cycles. In comparison, Zaker et al. [23] reported that ZSM-5 surface area decreased by >40% after a single use under similar reaction conditions as used here, with the main difference being water loading (50 wt% vs. 15 wt% here).

Table 3. *Surface area properties of ZSM-5 after use in catalytic cracking reactions calculated using the t-plot method.*

Catalyst	Micropore Area [m^2/g]	Micropore Volume [cc/g]	External Surface Area [m^2/g]	Correlation Coefficient
Fresh	293	0.15	60.2	0.99
Cycle 1	266	0.13	49.8	0.99
Cycle 2	230	0.11	40.5	0.98
Cycle 3	230	0.12	41.3	0.99
Cycle 4	236	0.12	36.6	0.98

SEM was used to evaluate changes in particle morphology after each use-regeneration cycle. **Figure 3** shows representative SEM images of the original material (Figure 3a) and catalyst after one (Figure 3b) and four use-regeneration cycles (Figure 3c); additional SEM images are located in **Figure S5** in the appendix, including images obtained from catalyst used for two and three use-regeneration cycles.

The native catalyst appears as an agglomerate of poorly defined nanoscale particles. One use-regeneration cycle results in a negligible change in the catalyst morphology, as shown in **Figure 3b**. After four use-regeneration cycles, the catalyst surface presents needle and flower-like features (Figure 3c). Maag et al. [26] previously described appearance of extensive needle-like features on the surface of ZSM-5 exposed to pure liquid or liquid-like supercritical water at the same temperature as used here for reaction, attributing their appearance to the ZSM-5 degradation process. In comparison with previous observations of ZSM-5 degradation made in pure water, the appearance of needle-like features is much less extensive in the presence of a reaction mixture containing 15 wt% water.

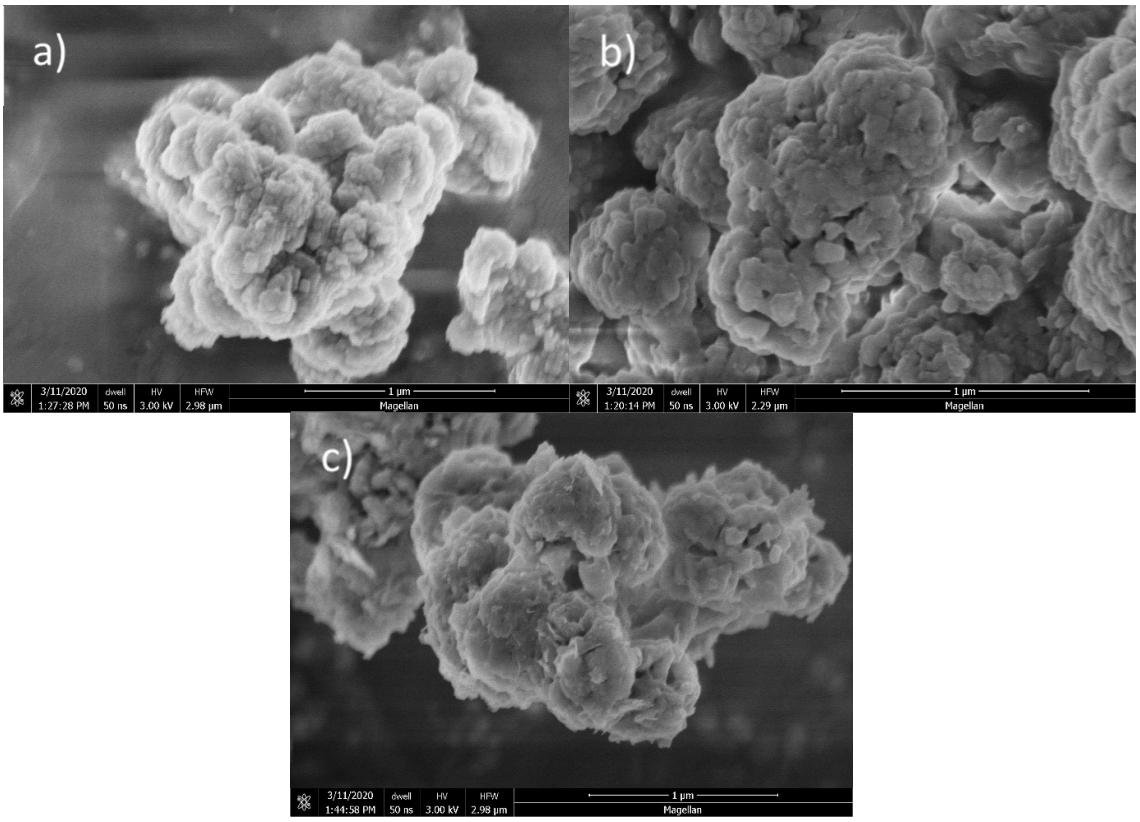

Figure 3. *Scanning electron microscope images of a) fresh calcined catalyst, b) cycle 1 catalyst, and c) cycle 4 catalyst.*

Brønsted acid sites (BAS) are the active sites for alkane cracking and aromatization reactions [[47-52] (Danuthai et al., Corma et al., Abbot, Tessennior et al., Bayense et al., Valle et al.)]. The aromatic yields reported after four use-regeneration cycles is indirect evidence of retained BAS density, since previous work showed that silicalite – which has no Brønsted acidity – failed to convert dodecane into aromatic products at similar conditions to those studied here [23]. To evaluate acid site chemistry in more detail, used-regenerated catalysts were studied using DRIFTS [26, 53]. **Figure 4** shows DRIFTS spectra obtained for the original catalyst material and catalyst after each of the four use-regeneration cycles. As expected, the original catalyst exhibits an intense band at approximately 3600 cm−1 associated with the Al−OH stretch indicating Brønsted acidity [54]. A second intense band at approximately 3750 cm^{-1} can be attributed to the Si−OH stretch of the silanol group.[54] After the first cycle, the

intensity of the feature attributed to Brønsted acidity decreases, and the intensity of a feature at 3650 cm^{-1} increases. The feature at 3650 cm^{-1} is attributable to extra-framework alumina (EFAL). Interestingly, the intensity of the silanol band may also decrease after the first use-regeneration cycle. In all subsequent cycles, both the BAS and EFAL feature are present, with the intensity of the BAS feature greater than that of the EFAL. The intensity of the silanol feature remains constant after decreasing after the first use-reuse cycle.

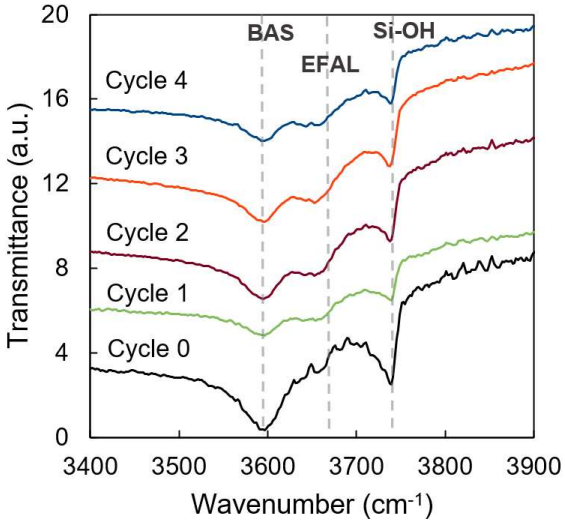

Figure 4. *DRIFTS spectra of calcined ZSM-5 catalyst at increasing usage.*

Conversion of BAS to EFAL is commonly observed as part of the dealumination process that removes acid sites from the zeolite framework [55]. Accordingly, the decreased intensity of the BAS feature and increased intensity of the EFAL feature after the first use-regeneration cycle is consistent with partial depletion of the original acid sites present on the catalyst. The persistence of the BAS feature after four use-regeneration cycles is consistent with retained acidity [54] and the observation of aromatic production (Figure 1). In comparison, Maag et al.[26] found that exposure to pure supercritical water at 400 °C resulted in nearly complete disappearance of the BAS feature from the DRIFTS spectrum, corresponding with >70% reduction of BAS density measured by titration methods.

The response silanol feature shown in **Figure 3** is worth further discussion. Silanol features are associated with defects in the zeolite lattice,[56] and are especially prominent at the surface [57]. Accordingly, the reduced intensity of the silanol band after the first use-regeneration cycle is consistent with the decreased surface area previously identified from measured N_2 isotherms. Stability of the silanol feature after subsequent use-regeneration cycles is therefore consistent with the aforementioned stability of textural properties.

In summary, four use-regeneration cycles of ZSM-5 in the presence of a minority water phase resulted in modest (<20%) reductions in activity and surface area, in parallel with some qualitative changes in surface morphology and BAS density revealed by DRIFTS. Prior work by Mo et al.[31] of palmitic acid cracking with a majority water component (66 wt%) did not report extensive characterization data, making difficult direct comparison with the results presented here. The most appropriate comparison is the work reported by Zaker et al.[23], performed in a reaction mixture consisting of 50 wt% water and 50 wt% dodecane. Compared with the previous work by Zaker et al.[23], using ZSM-5 in the presence of a minority water phase (15 wt%) resulted in much less degradation, indicating much greater potential for commercial use. More, extending zeolite structural and acid site stability came in parallel with increased activity (as shown in Table 2) and without excessive coke formation. These positive findings motivate follow-on studies to examine the cracking and aromatization reaction in greater detail.

Reaction Pathway

Experiments at both “hydrothermal” (SCW with no catalyst) conditions and catalytic conditions were conducted to better understand unique contributions to the reaction. Representative GC/FID spectra for hydrothermal and catalytic cracking products can be seen in **Figure S6** in the appendix. Hydrothermal conversion of PA (no catalyst, 15 wt% water, 23 ± 1 MPa and 400 C held for 30 minutes) resulted in complete conversion within detection limits

a produced straight chain paraffins and relatively few straight chain olefins. Mass spectrometry showed signs of straight-chain carboxylic acids, suggesting that decarboxylation and chain cracking are occurring simultaneously.

The high conversion of palmitic acid observed in SCW without catalyst is interesting considering lack of conversion reported for hexadecane in SCW at similar conditions [REFs]. It's clear that the carboxylic acid group is responsible for the high conversion observed, in line with work on hexyl-sulfide decomposition in SCW in which the alkane analog is unreactive [58]. Zaker et al.[23] found that in SCW-dodecane cracking with just SCW and with SCW, nitric acid, and silicalite framework, dodecane was unreactive. Therefore, it seems that SCW alone nor SCW with a strong acid present does not offer appropriate acid sites to imitate the carbocation isomerization and aromatization present with ZSM-5. From this and the product distribution, it seems that a radical pathway is responsible for decomposition without the presence of catalyst, with a rate which is not able to be neglected.

Prior research has identified the role of carbocation intermediates in cracking reactions with zeolites [43, 59]. Catalytic cracking of PA produced significant yields of aromatic compounds as well as of branched and cyclic paraffins and olefins, clearly demonstrating a catalytic pathway to isomerization and aromatization when juxtaposed against hydrothermal products. However, while the system has catalyst present, there is likely also radical thermal decomposition occurring outside of the catalyst.

Figure 5 shows the overall carbon yield breakdown of products over increasing temperature and reaction times. Aromatic yield increases with time even after PA is entirely converted. Combined with the decrease of aliphatics over the same time range, it is clear that aliphatics are being converted to aromatics.

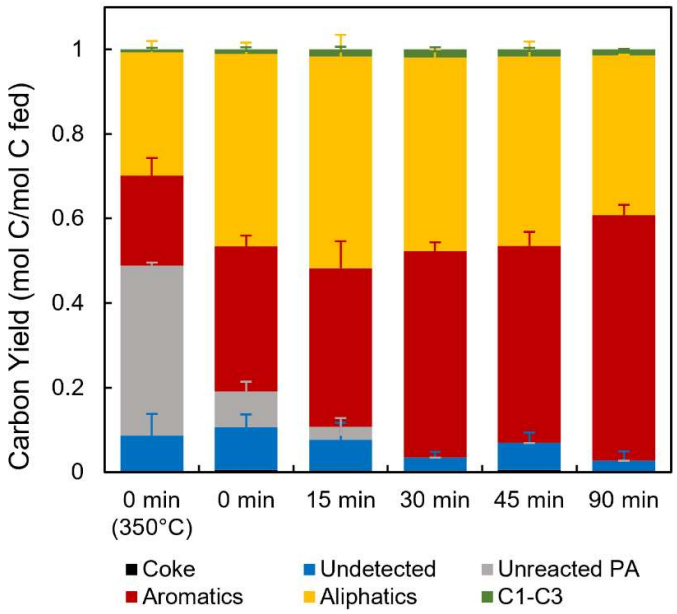

Figure 5. *Overall carbon yield of all products at varying reaction times.*

To search for a primary precursor to aromatic formation, aliphatic yields were analyzed in more detail in **Figure 6**.

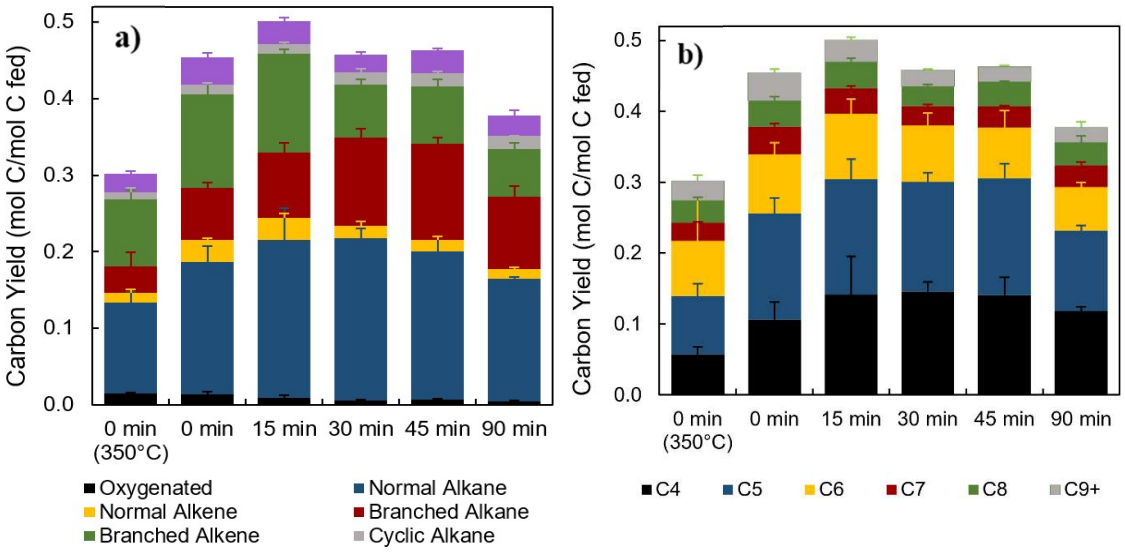

Figure 6. *Aliphatic yield by a) compound type and b) carbon number.*

Oxygenated aliphatics and branched alkenes are saturated by hydrogen from aromatization reactions over time, forming the trend of increasing alkanes and decreasing alkenes observed in **Figure 6a**. From 30 to 90 minutes, after complete PA conversion, aliphatic conversion

decrease by 80.5 ± 16.6 mmol C/mol C fed (mmol C yield), on par with the 91.5 ± 32.5 mmol C yield increase in aromatics over the same duration; this decrease may be entirely attributed to a C4-C6 decrease of 87.1 ± 29.2 mmol C yield from 30 to 90 minutes while C7-C8 increased by 7.9 ± 14.9 mmol C yield. From this it likely seems straight-chain C4-C6 aliphatics are undergoing addition reactions to from aromatics and potentially also C7-C8 aliphatic isomers. This is agrees with previous literature: Y. Ono et al [60] reacted pentanes over HZSM-5 to find that light olefins and C4 and C5 hydrocarbons acted as intermediates for aromatics while others have hypothesized that light olefins (C2-C4) serve as intermediates [60, 61]. While the data is sufficient to explain aromatic formation after complete PA conversion, the temporal aspect of these reactions suggest they are not the primary pathway as previous aromatic formation occurs much more rapidly.

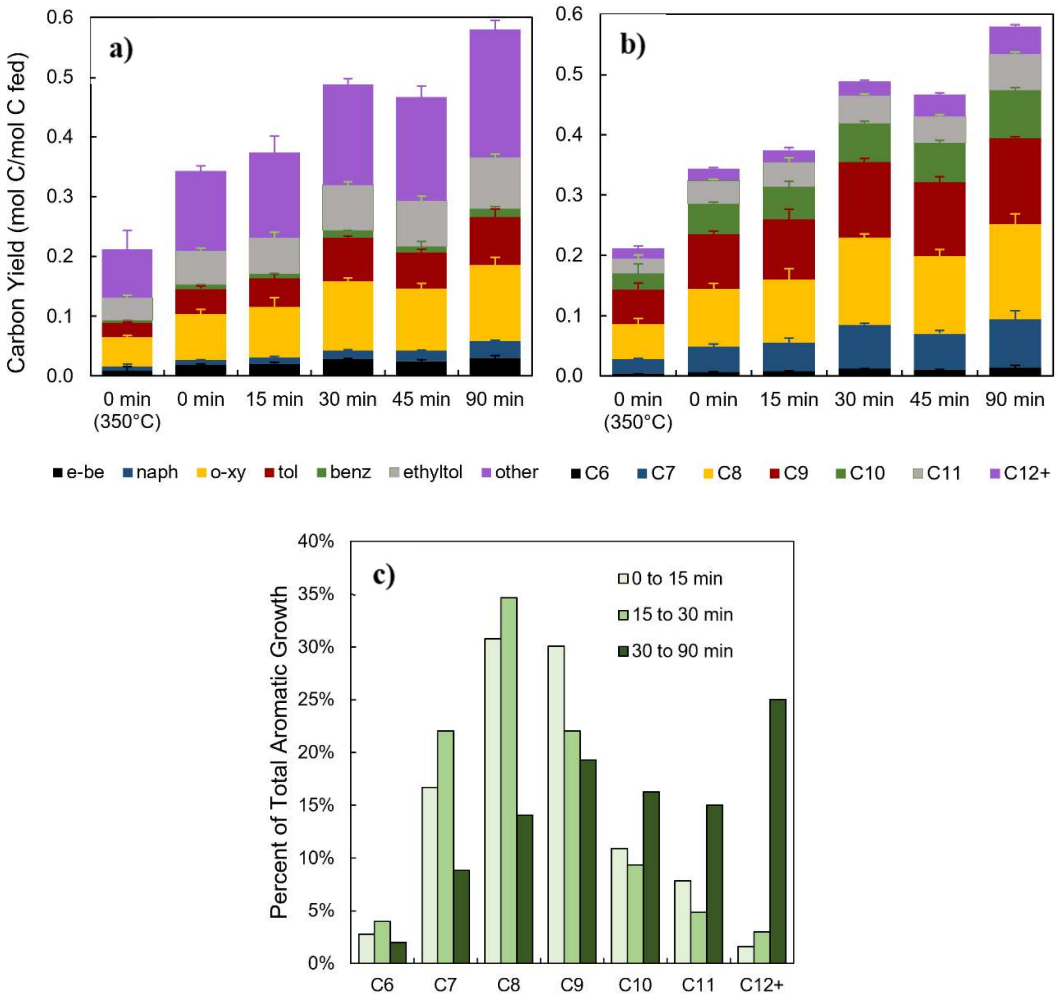

Figure 7. *Aromatic yield by c) compound type d) carbon number, and c) by increase between time points.*

To better understand the reactions that may be taking place, an aromatic carbon balance was investigated in **Figure 7**. The aromatics which are formed between 0 to 30 minutes are not the primary aromatics being formed between 30 to 90 minutes, as can be seen in **Figure 7c**. From 15 to 30 minutes, C_{10+} aromatic increase by 20 mmol C yield while aromatics overall increase by 114 mmol C yield, representing 17% of the total increase, while C7-C8 aromatics represent 57%. From 30 to 90 minutes, C_{10+} aromatics constitute 56% of the aromatic carbon growth of 91 mmol C yield while C_7-C_8 constitute only 23%. Therefore, it appears that C_4-C_6 aliphatic additions and aromatization represent a slow, secondary pathway to aromatic

formation separate from the primary pathway undertaken in the reaction while PA is present. The primary pathway appears to be related directly to the presence of PA due to the dramatic slow in aromatic production once PA is completely reacted, and therefore may be linked to intermediates formed as PA cracks on the surface of the catalyst. An alternative perspective may consider reduction of catalytic activity as coke forms on the catalyst surface reducing rates of aromatic production, but this is unlikely as coking remains much lower than other studies have shown while maintaining catalytic activity. **Figure 8** details a proposed reaction pathway which encompasses this information.

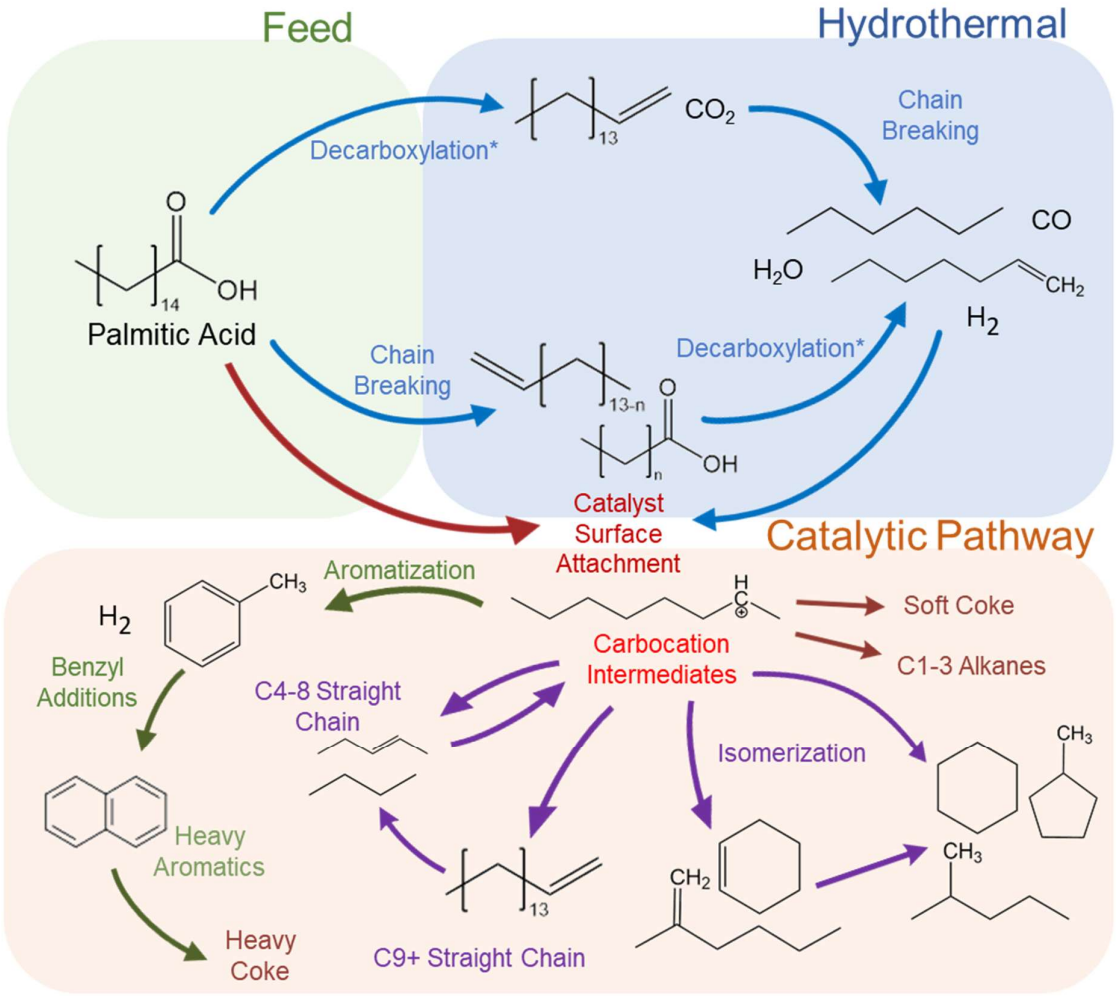

Figure 8: *Overall reaction pathway showing classes of compounds formed through the cracking of palmitic acid (neglecting relative yields).*

Conclusion

Findings and Future Work

Within this work, it has been shown that ZSM-5 can convert palmitic acid to desired aromatics and olefins at superior rates and with less catalyst loading, degradation, and coking than previously found [31]. Added catalyst stability and coking is achieved through a lower water load which has been shown within previous works to decrease effects of coking and catalyst degradation [23, 24, 26]. Many findings in this work coincide with findings from previous works, including the importance of Brønsted acid sites for PA conversion and aromatization. Interestingly, it was found that catalyst activity decreased with the first reuse but increased slightly after subsequent uses. This can be attributed to catalyst degradation allowing access to pores previously blocked by prior degradation, increasing catalytic activity overall. It was demonstrated that ZSM-5 can be recycled for use at least four times retaining the vast majority of its activity and structural integrity. The reaction pathway of palmitic acid cracking was also investigated in this work. While there does not appear to be a specific precursor to aromatic formation from product analysis at various reaction times/conversions, a secondary pathway appears to occur after complete conversion of PA from 30 to 90 minutes in which C_{4-6} addition and dehydroaromatization appears to be occurring to form a higher ratio of heavier aromatics (C_{10+}). This work shows that having a minority weight content of water can be beneficial to the upgrading of an abundant fatty acid by increasing the catalyst's lifetime through coke suppression and minimal structural changes. Further work could explore the use of this strategy for the upgrading of other fatty acids and waste oils, and more work can be applied to further understanding catalytic and hydrothermal contributions to the reaction pathway.

Acknowledgements

Michael Timko provided guidance and helped perform analysis.

Sanket Sabnis and Wei Fan from University of Massachusetts Amherst took SEM images and provided analysis of those images.

Professor Bond from Syracuse University helped with feedback on pathway discussion.

Azedah Zaker helped provide guidance and data analysis.

Geoffrey Thompsett for help around the lab and assisted with collection of the nitrogen adsorption data. Andy Butler for help with use of the TPO and preparing samples for NMR.

Heather LeClerc for help around the lab, editing, and collecting XRD data.

Cameron Armstrong for helping with the XRD data collection.

Feng Chang for help around the lab and help troubleshooting the GC.

References

1. Hussain, A., S.M. Arif, and M. Aslam, *Emerging renewable and sustainable energy technologies: State of the art.* Renewable and Sustainable Energy Reviews, 2017. **71**(Generic): p. 12-28.
2. Lin, Z., V. Nikolakis, and M. Ierapetritou, *Life cycle assessment of biobased p -xylene production.* Industrial and Engineering Chemistry Research, 2015. **54**(8): p. 2366-2378.
3. Harmsen, P.F.H., M.M. Hackmann, and H.L. Bos, *Green building blocks for bio-based plastics.* Biofuels Bioproducts and Biorefining, 2014. **8**(3): p. 306-324.
4. Vlysidis, A., et al., *A techno-economic analysis of biodiesel biorefineries: Assessment of integrated designs for the co-production of fuels and chemicals.* Energy, 2011. **36**(8): p. 4671-4683.
5. Botas, J.A., et al., *Catalytic conversion of rapeseed oil for the production of raw chemicals, fuels and carbon nanotubes over Ni-modified nanocrystalline and hierarchical ZSM-5.* Applied Catalysis B: Environmental, 2014. **145**: p. 205-215.
6. Emori, E.Y., et al., *Catalytic cracking of soybean oil using ZSM5 zeolite.* Catalysis Today, 2017. **279**: p. 168-176.
7. Ong, Y.K. and S. Bhatia, *The current status and perspectives of biofuel production via catalytic cracking of edible and non-edible oils.* Energy, 2010.
8. Katikaneni, S.P.R., J.D. Adjaye, and N.N. Bakhshi, *Studies on the Catalytic Conversion of Canola Oil to Hydrocarbons: Influence of Hybrid Catalysts and Steam.* Energy & Fuels, 1995. **9**(4): p. 599-609.
9. Katikaneni, S.P.R., J.D. Adjaye, and N.N. Bakhshi, *Catalytic conversion of canola oil to fuels and chemicals over various cracking catalysts.* The Canadian Journal of Chemical Engineering, 1995. **73**(4): p. 484-497.
10. Twaiq, F.A., A.R. Mohamed, and S. Bhatia, *Liquid hydrocarbon fuels from palm oil by catalytic cracking over aluminosilicate mesoporous catalysts with various Si/Al ratios.* Microporous and Mesoporous Materials, 2003. **64**(1): p. 95-107.
11. Zhang, H., et al., *Catalytic conversion of biomass-derived feedstocks into olefins and aromatics with ZSM-5: the hydrogen to carbon effective ratio.* Energy & Environmental Science, 2011. **4**(6): p. 2297-2307.
12. Bibby, D.M., et al., *Coke formation in zeolite ZSM-5*. 1986. p. 493-502.

13. Milina, M., et al., *Mesopore quality determines the lifetime of hierarchically structured zeolite catalysts.* Nature Communications, 2014. **5**(May).
14. Milina, M., S. Mitchell, and J. Pérez-Ramírez, *Prospectives for bio-oil upgrading via esterification over zeolite catalysts*. 2014. p. 176-183.
15. Taufiqurrahmi, N., A.R. Mohamed, and S. Bhatia, *Production of biofuel from waste cooking palm oil using nanocrystalline zeolite as catalyst: Process optimization studies.* Bioresource Technology, 2011.
16. Abbasov, V., et al., *Catalytic cracking of vegetable oils and vacuum gasoil with commercial high alumina zeolite and halloysite nanotubes for biofuel production.* Fuel, 2016. **181**: p. 55-63.
17. Hew, K.L., et al., *Catalytic cracking of bio-oil to organic liquid product (OLP).* Bioresource Technology, 2010. **101**(22): p. 8855-8858.
18. Leng, T.Y., A.R. Mohamed, and S. Bhatia, *Catalytic conversion of palm oil to fuels and chemicals.* The Canadian Journal of Chemical Engineering, 1999. **77**(1): p. 156-162.
19. Prado, C.M.R. and N.R. Antoniosi Filho, *Production and characterization of the biofuels obtained by thermal cracking and thermal catalytic cracking of vegetable oils.* Journal of Analytical and Applied Pyrolysis, 2009. **86**(2): p. 338-347.
20. Sang, O.Y., *Biofuel Production from Catalytic Cracking of Palm Oil.* Energy Sources, 2003. **25**(9): p. 859-869.
21. Sharma, R.K. and N.N. Bakhshi, *Upgrading of tall oil to fuels and chemicals over HZSM-5 catalyst using various diluents.* The Canadian Journal of Chemical Engineering, 1991. **69**(5): p. 1082-1086.
22. Tamunaidu, P. and S. Bhatia, *Catalytic cracking of palm oil for the production of biofuels: Optimization studies.* Bioresource Technology, 2007. **98**(18): p. 3593-3601.
23. Zaker, A., et al., *Evidence of heterogeneous catalytic activity of ZSM-5 in supercritical water for dodecane cracking.* Catalysis Today, 2018. **317**(May): p. 2-11.
24. Guerra, P., et al., *Analysis of coke formed during zeolite-catalyzed supercritical dodecane cracking: Effect of supercritical water*. 2020. p. 117330.
25. Maag, A.R., et al., *Comparative study of gaseous and high-pressure liquid reactions in industrial chemistry*. 2019. p. 107661.
26. Maag, A.R., et al., *ZSM-5 decrystallization and dealumination in hot liquid water.* Physical Chemistry Chemical Physics, 2019.

27. Zhang, L., et al., *Factors that Determine Zeolite Stability in Hot Liquid Water.* Journal of the American Chemical Society, 2015. **137**(36): p. 11810-11819.
28. Ravenelle, R.M., et al., *Stability of zeolites in hot liquid water.* Journal of Physical Chemistry C, 2010.
29. Wang, I., et al., *The comparison of cracking activity, product selectivity, and steam stability of ZSM-5 to other cracking catalysts*. 1979. p. 140-147.
30. Gardner, D.W., et al., *Insights into the Hydrothermal Stability of ZSM-5 under Relevant Biomass Conversion Reaction Conditions.* ACS Catalysis, 2015. **5**(7): p. 4418-4422.
31. Mo, N. and P.E. Savage, *Hydrothermal Catalytic Cracking of Fatty Acids with HZSM-5.* ACS Sustainable Chemistry & Engineering, 2014. **2**(1): p. 88-94.
32. Groen, J.C., et al., *Mesoporous beta zeolite obtained by desilication*. 2008. p. 93-102.
33. Kooyman, P.J., P. van der Waal, and H. van Bekkum, *Acid dealumination of ZSM-5*. 1997. p. 50-53.
34. Ogura, M., et al., *Alkali-treatment technique — new method for modification of structural and acid-catalytic properties of ZSM-5 zeolites*. 2001. p. 33-43.
35. Savage, P.E., *Organic Chemical Reactions in Supercritical Water.* Chemical Reviews, 1999. **99**(2): p. 603-622.
36. Deepa, A.K. and P.L. Dhepe, *Lignin Depolymerization into Aromatic Monomers over Solid Acid Catalysts.* ACS Catalysis, 2015. **5**(1): p. 365-379.
37. Liu, M., et al., *Upgrading of palmitic acid and hexadecanamide over Co-based catalysts: Effect of support (SiO2, Γ-Al2O3 and H-ZSM-22).* Catalysis Communications, 2019.
38. He, P. and A.F. Ghoniem, *A Group Contribution Pseudocomponent Method for Phase Equilibrium Modeling of Mixtures of Petroleum Fluids and a Solvent.* Industrial & Engineering Chemistry Research, 2015. **54**(35): p. 8809-8820.
39. Perkins, G., R.E. Laramy, and L.D. Lively, *Flame Response in the Quantitative Determination of High Molecular Weight Paraffins and Alcohols by Gas Chromatography.* Analytical Chemistry, 1963. **35**(3): p. 360-362.
40. Class, C.A., et al., *Detailed kinetic model for hexyl sulfide pyrolysis and its desulfurization by supercritical water.* Physical Chemistry Chemical Physics, 2019. **21**(20): p. 10311-10324.
41. McHugh, M. and V. Krukonis, *Supercritical fluid extraction: practice and purpose*. Second ed. 2013: Elsevier.

42. Wagner, W. and A. Pruß, *The IAPWS Formulation 1995 for the Thermodynamic Properties of Ordinary Water Substance for General and Scientific Use.* Journal of Physical and Chemical Reference Data, 2002. **31**(2): p. 387-535.
43. Santos, M.R., et al., *Catalytic cracking of palmitic and oleic acids pre-adsorbed on γ-alumina.* Catalysis Today, 2019(May 2018): p. 1-6.
44. Zapata, P.A., et al., *Silylated hydrophobic zeolites with enhanced tolerance to hot liquid water*. 2013. p. 82-97.
45. Nandiwale, K.Y., et al., *Catalytic upgrading of renewable levulinic acid to ethyl levulinate biodiesel using dodecatungstophosphoric acid supported on desilicated H-ZSM-5 as catalyst*. 2013. p. 90-98.
46. ASTM, *D5758-01* 2011, ASTM International p. 3-5.
47. Corma, A., et al., *The role of different types of acid site in the cracking of alkanes on zeolite catalysts.* Journal of Catalysis, 1985. **93**(1): p. 30-37.
48. Danuthai, T., et al., *Conversion of methylesters to hydrocarbons over an H-ZSM5 zeolite catalyst.* Applied Catalysis A: General, 2009. **361**(1-2): p. 99-105.
49. Abbot, J., *Role of Brønsted and Lewis acid sites during cracking reactions of alkanes.* Applied Catalysis, 1989. **47**(1): p. 33-44.
50. Bayense, C.R., A.J.H.P. van der Pol, and J.H.C. van Hooff, *Aromatization of propane over MFI-gallosilicates.* Applied Catalysis, 1991. **72**(1): p. 81-98.
51. Tessonnier, J.-P., et al., *Methane dehydro-aromatization on Mo/ZSM-5: About the hidden role of Brønsted acid sites.* Applied Catalysis A: General, 2008. **336**(1-2): p. 79-88.
52. Valle, B., et al., *Hydrothermally stable HZSM-5 zeolite catalysts for the transformation of crude bio-oil into hydrocarbons.* Applied Catalysis B: Environmental, 2010. **100**(1-2): p. 318-327.
53. Kumar, V.V., et al., *Role of Brønsted and Lewis acid sites on Ni/TiO2 catalyst for vapour phase hydrogenation of levulinic acid: Kinetic and mechanistic study.* Applied Catalysis A: General, 2015. **505**: p. 217-223.
54. Datka, J., et al., *Physicochemical and Catalytic Properties of HZSM-5 Zeolites Dealuminated by the Treatment with Steam.* The Journal of Physical Chemistry, 1996. **100**(34): p. 14451-14456.
55. Loeffler, E., et al., *Study of different states of nonframework aluminum in hydrothermally dealuminated HZSM-5 zeolites using diffuse reflectance i.r. spectroscopy.* Zeolites, 1990. **10**(4): p. 266-271.

56. Ye, Y., et al., *Influence of Silanol Defects of ZSM-5 Zeolites on Trioxane Synthesis from Formaldehyde.* Catalysis Letters, 2020. **150**(5): p. 1445-1453.
57. Barbera, K., et al., *Structure–deactivation relationship for ZSM-5 catalysts governed by framework defects.* Journal of Catalysis, 2011. **280**(2): p. 196-205.
58. Kida, Y., et al., *Combining experiment and theory to elucidate the role of supercritical water in sulfide decomposition.* Physical Chemistry Chemical Physics, 2014. **16**(20): p. 9220-9228.
59. Kotrel, S., H. Knözinger, and B.C. Gates, *The Haag-Dessau mechanism of protolytic cracking of alkanes.* Microporous and Mesoporous Materials, 2000.
60. Sirokman, G., Y. Sendoda, and Y. Ono, *Conversion of pentane into aromatics over ZSM—5 zeolites.* Zeolites, 1986. **6**(4): p. 299-303.
61. Scurrell, M.S., *Factors affecting the selectivity of the aromatization of light alkanes on modified ZSM-5 catalysts.* Applied Catalysis, 1988. **41**: p. 89-98.
62. Wisniewski, A., et al., *Biofuels from waste fish oil pyrolysis: Chemical composition.* Fuel, 2010. **89**(3): p. 563-568.

Appendix

This appendix contains: 1) Reaction diagram 2) Detailed catalyst characterization methods 3) Unknown compounds elemental balance 3) Comparison of aromatic rate production 4) NMR of heavy cracking products 5) SEM Images of re-used catalyst 6) Representative GC spectra of thermal and catalytic products. 7) TPO of used catalyst

A1. Reaction Diagram

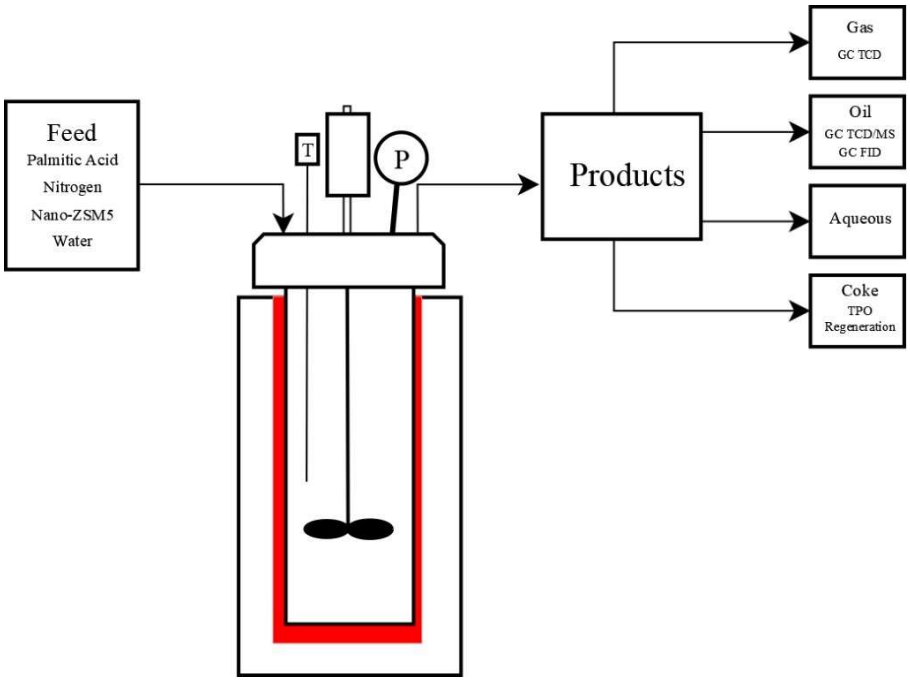

Figure S1. *Reaction schematic for catalytic cracking reactions.*

A2. Catalyst Characterization Techniques

Diffuse Reflectance Infrared Fourier Transform Spectroscopy (DRIFT) was performed using a Nicolet Magna IR 560 spectrometer and a SpectraTech DRIFTS cell. The method based on the DRIFTS method from Maag et al.[26] The cell was loaded with ZSM-5 before being purged with N2 for 10 minutes to remove ambient CO_2. The temperature was increased in 20 °C increments at 10-15 min intervals until 100 °C, where it was held for 30 minutes before increasing in 50 °C increments until reaching 550 °C. Samples were analyzed over the range from 4000 to 600 cm−1 , at a resolution of 2 cm−1 , and an accumulation of 256 scans at 550 °C.

The X-Ray Powder Diffraction (XRD) patterns were taken using a Rigaku X-ray diffractometer with Cu Kα radiation at 37.5 keV and 25 mA. A scan rate of 0.05° (2θ) per second over a 6 theta to 80 range was used. XRD patterns were analyzed using MDI Jade software. The degree of crystallinity was calculated using the ASTM Standard D5758 [46].

N2 Adsorption was performed using a Quantachrome autosorb IQ to determine catalyst surface area and micropore volume. Zeolite samples (~0.1 g) were added to a glass bulb and degassed at a temperature ramp of 2 ºC min^{-1} with 30 min temperature holds at 80 and 120 ºC before increasing to 350 ºC for 420 min. Analysis was performed by dosing the sample with nitrogen as the adsorbate and cooling the sample with liquid nitrogen. 43 isothermal P/P_0 points were obtained between 0.00013 and 1 followed by 16 desorption points from 1 to 0.1. Micropore and external surface area were determined by applying the DR method to model the adsorption isotherm between P/P_0 of 0.15 to 0.95.

A3. Comparative Aromatic Rate Production

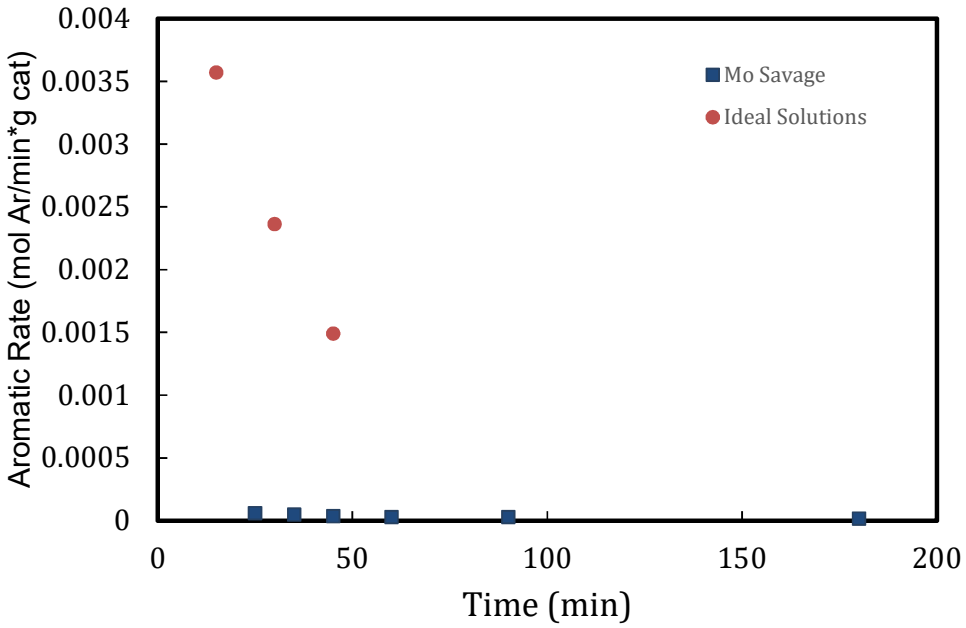

Figure S2. Comparison of the rates of producing aromatic compounds from data in this study and Mo et al. [31]

A4. ^{1}H NMR of heavy oil products

To analyze "heavy" oil-phase products, referring to compounds which are non-volatile within the parameters of our gas chromatography analysis, we performed ambient evaporation-to-dryness within a fume hood for 3 weeks. The resulting oil phases were then analyzed with proton NMR, the results of which can be seen in **Figures S3 and S4**.

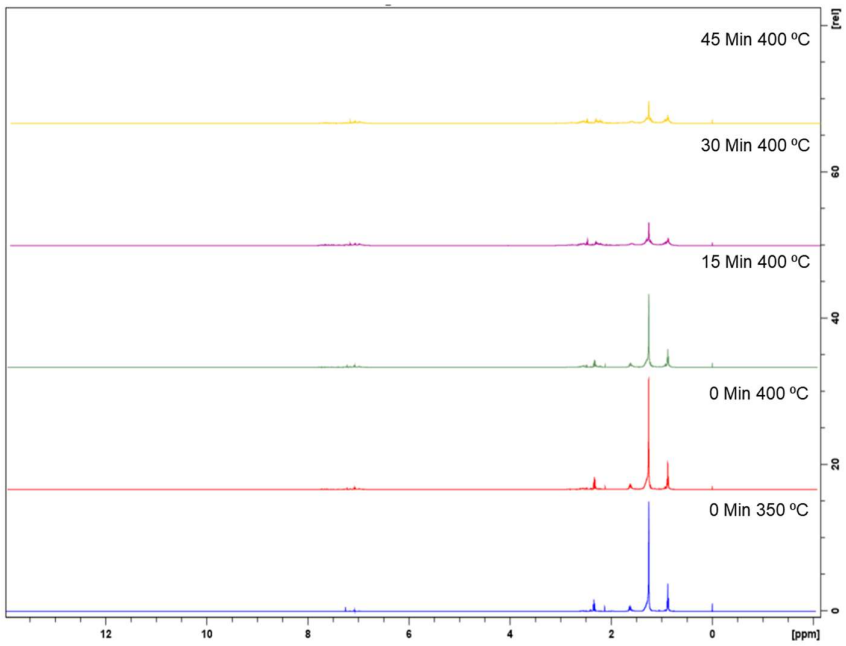

Figure S3: *Proton NMR data for "heavy oil" products, acquired through evaporation-to-dryness for 3 weeks inside of a fume hood of product oil phase. Integrations of peaks can be found in Figure S4 below.*

Integration was performed on the NMR shifts found in graph **S3.** Each peach represents a hydrogen on a different functional group. For the purposes of this study the shifts between 0.5 and 2.5 ppm are consider aliphatic hydrogen, shifts between 2.5 and 3 ppm are consider aliphatic hydrogen attached to an aromatic molecule and shifts between 7 and 9 ppm are considered aromatic[62]. The area of the aliphatic peaks and the area aromatic peaks were divided by the total area to get the area fraction which is plotted in **Figure S4**. It is noteworthy that no peaks were found in the 11-12 ppm range which is generally expected for oxygenated compounds.

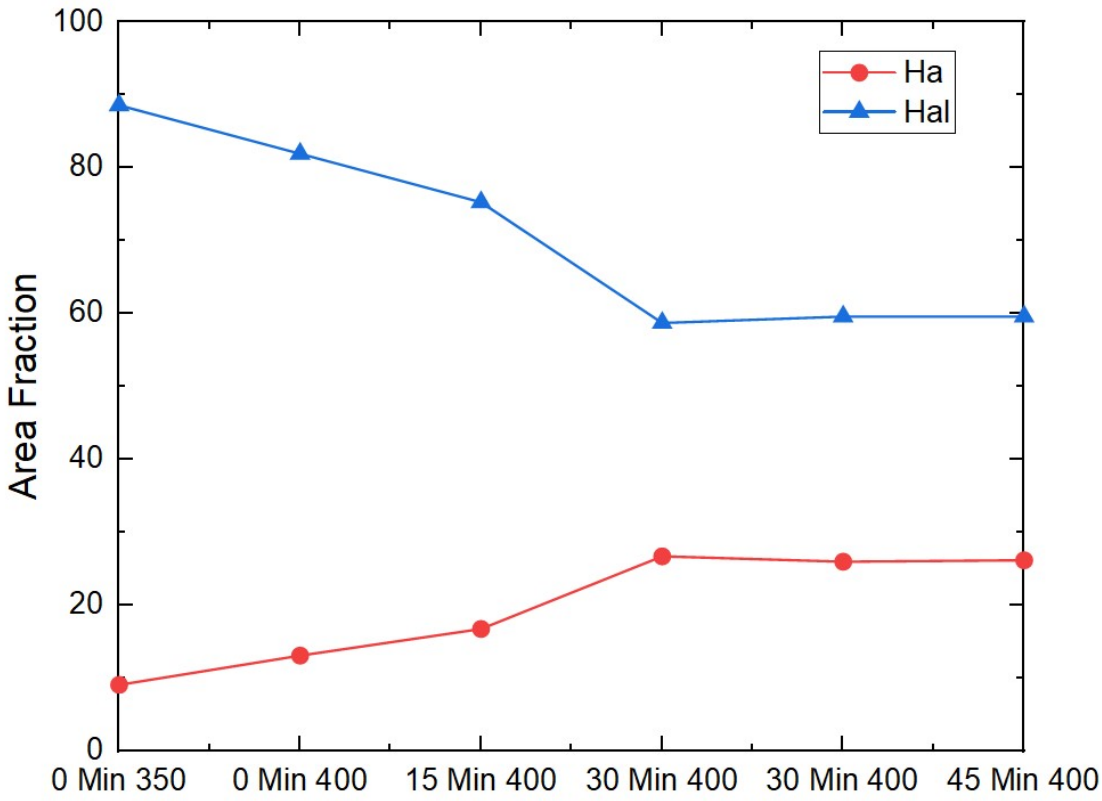

Figure S4: *NMR peak area of the of aliphatic hydrogen and aromatic divide by the total area of all the peaks plotted at each reaction time point. 'Hal' represents aliphatic hydrogen and 'Ha' represents aromatic hydrogen.*

A5. SEM images of used catalysts

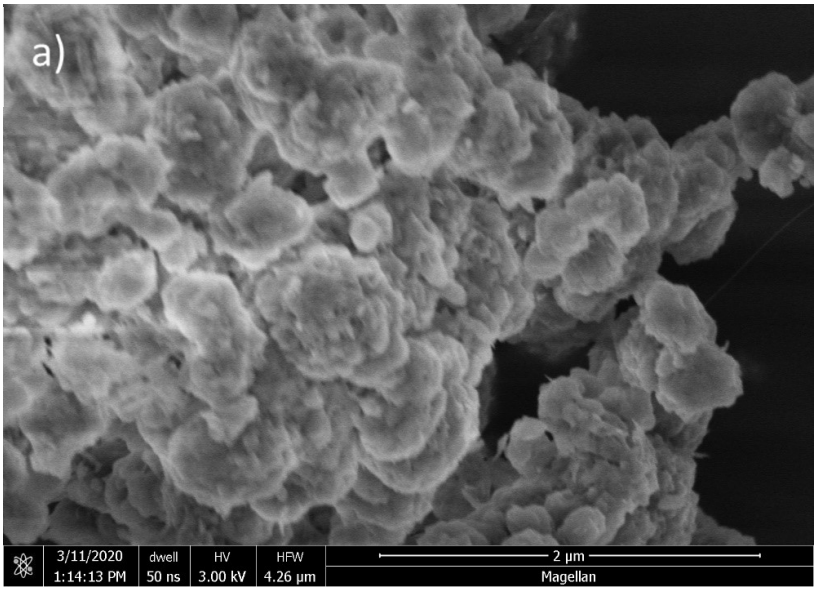

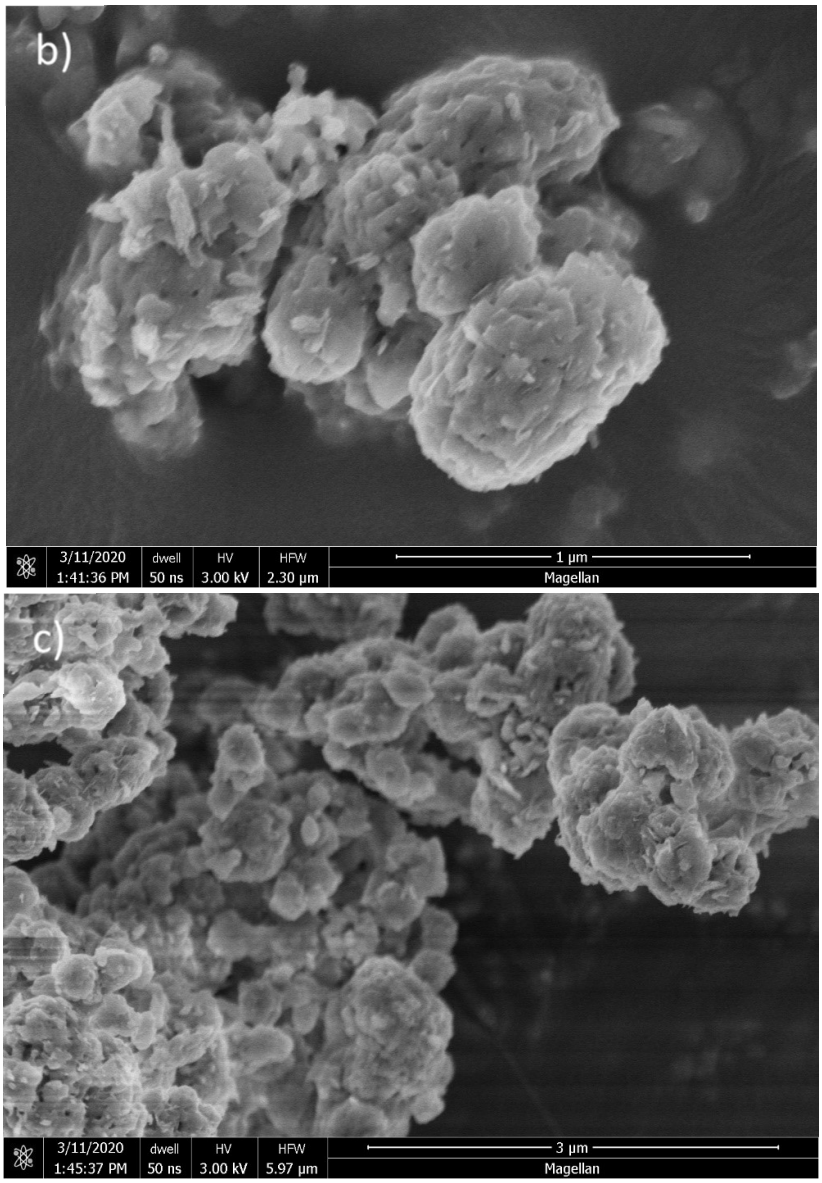

Figure S5. *Additional SEM images of used catalysts. Image a) cycle 2 catalyst, b) cycle 3 catalyst, c) lower magnification image of cycle 4 catalyst.*

A6. Representative GC spectra of thermal and catalytic cracking reactions

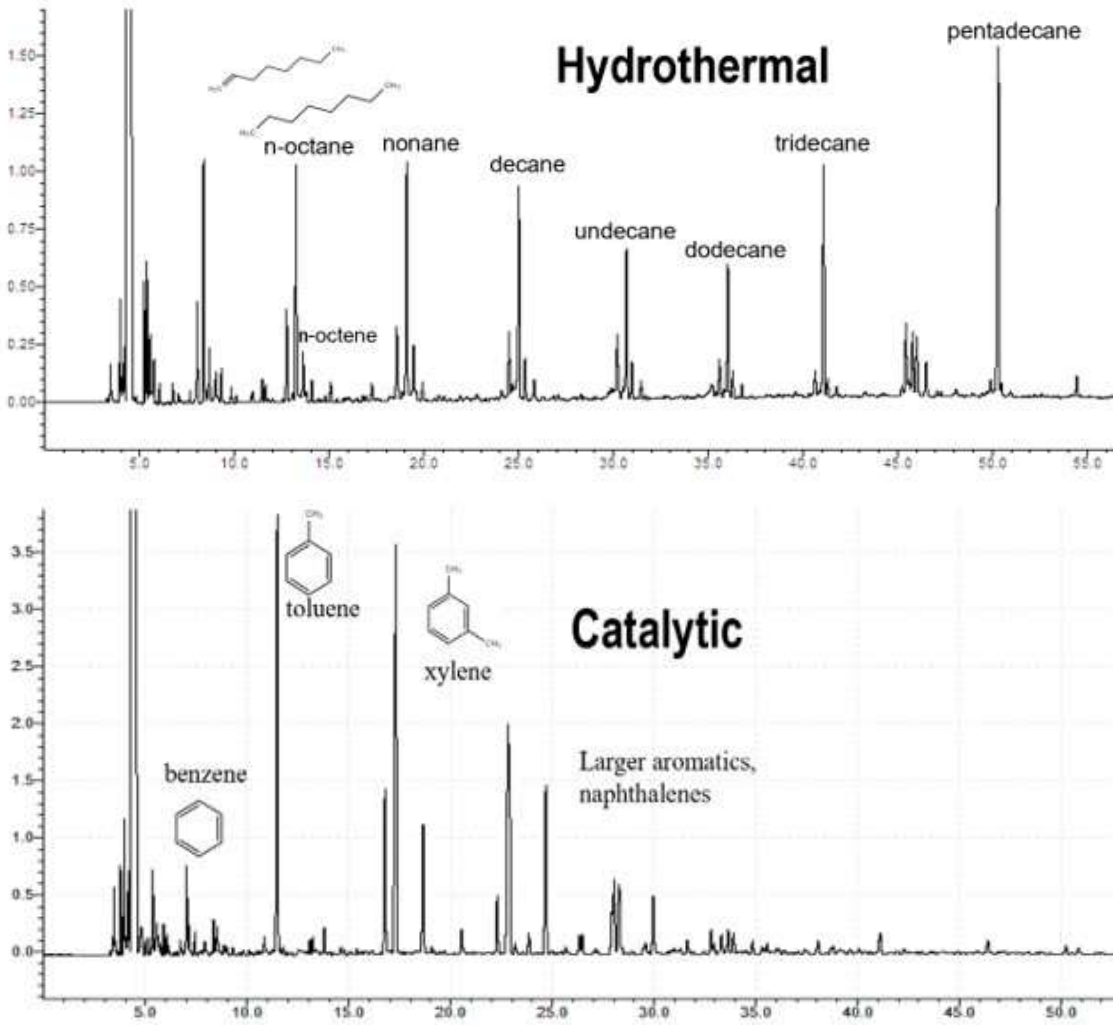

Figure S6: *Representative mass spectra for hydrothermal (SCW, no catalyst, 30 minutes, 400°C) and catalytic (SCW, 5 wt% catalyst, 30 minutes, 400°C) oil phase products. Hydrothermal conversion of PA was 100% within detection limits in 30 minutes, yielding mostly straight-chain alkanes and essentially no aromatics or isomer hydrocarbons. Catalytic conversion of PA reached similar conversion in 30 minutes, yielding a variety of aromatics and hydrocarbon isomers.*

A7. Thermal Profile Oxidation (TPO) of Coke

To analyze and quantify coke production, TPO, a form of thermogravimetric analysis (TGA), was used. Equipment and parameters used for TPO can be found in the Materials and Methods section, and thermographs can be found below.

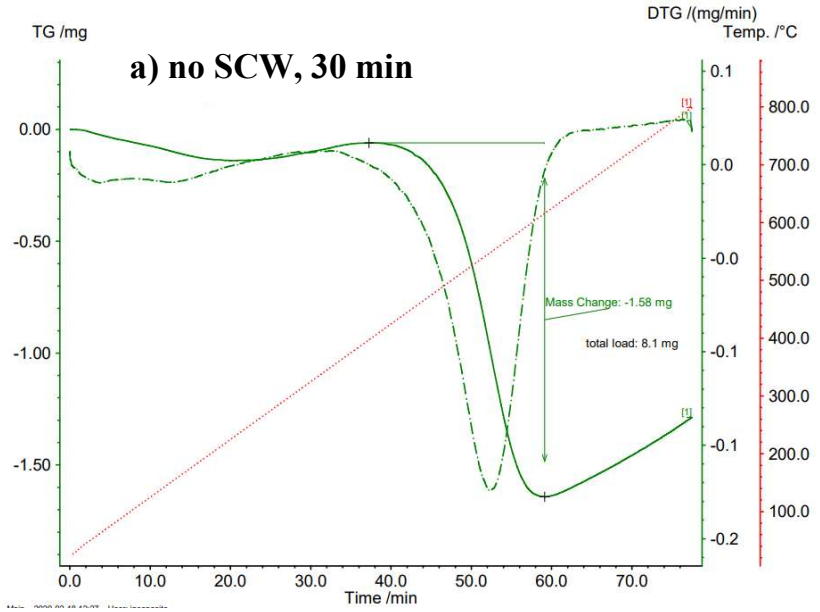
a) no SCW, 30 min
TG /mg
DTG /(mg/min)
Temp. /°C
Mass Change: -1.58 mg
total load: 8.1 mg
Time /min

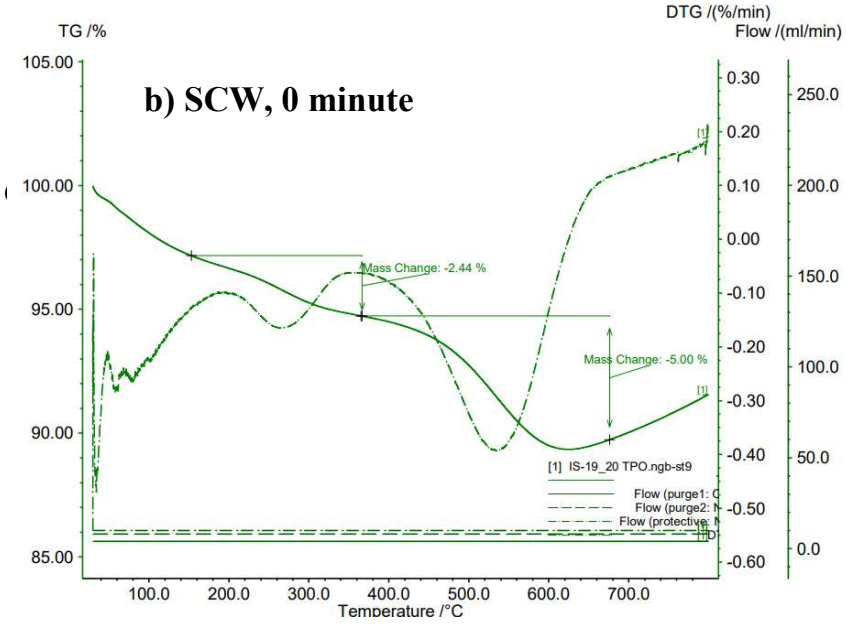
b) SCW, 0 minute
TG /%
DTG /(%/min)
Flow /(ml/min)
Mass Change: -2.44 %
Mass Change: -5.00 %
[1] IS-19_20 TPO.ngb-st9
Temperature /°C

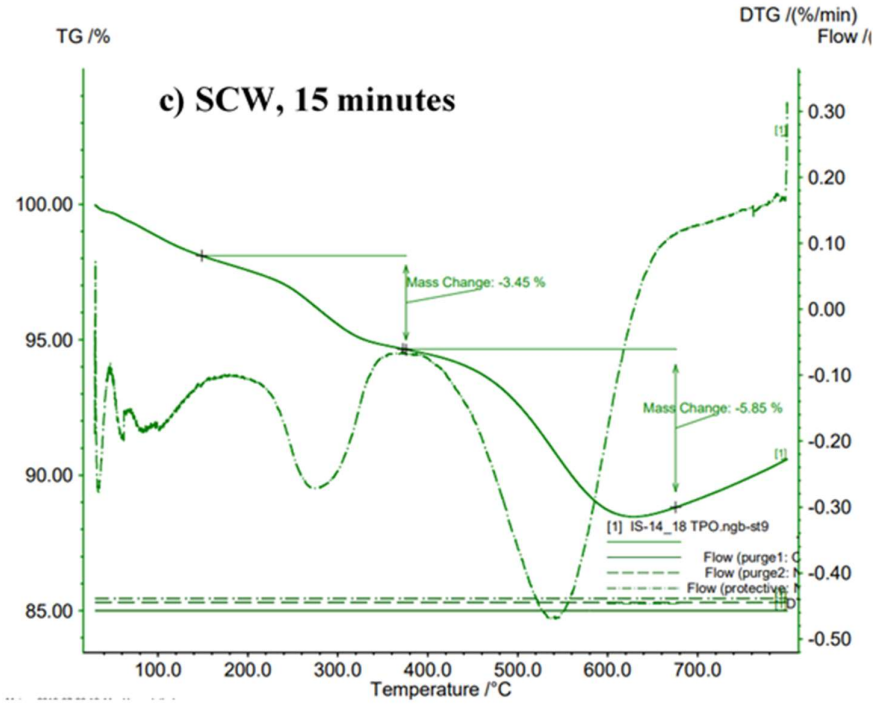

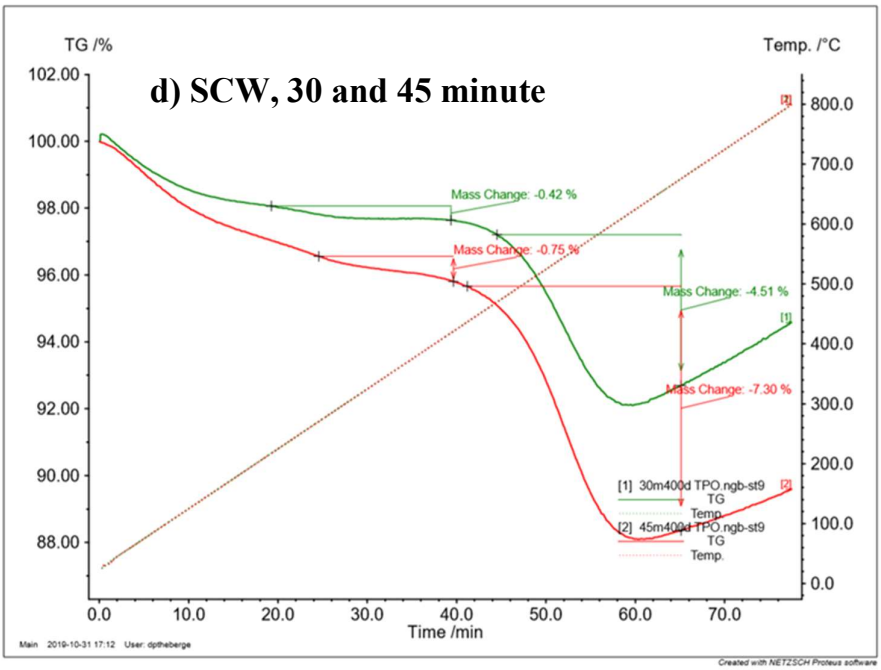

Figure S7: *TPO thermographs of coke for the following PA cracking reaction conditions (all at 400°C, 22 ± 2 MPa):(a) no SCW with catalyst (5 wt%) for 30 minutes, and the rest with 15 wt% SCW for (b) 0 minutes, (c) 15 minutes, (d) 30 [green] and 45 [red] minutes.*